A CONVECTIVE HEAT TRANSFER STUDY ON THE STRONGLY CONCAVE SURFACE OF A FILM COOLED TURBINE ROTOR BLADE

C. CAMCI *
The Pennsylvania State University
Aerospace Engineering Department
University Park, PA 16802

ABSTRACT

A short duration heat transfer study of discrete hole film cooling on the strongly concave pressure side of a high pressure turbine blade is presented. Numerous past investigations showed that, streamwise curvature in the plane of mean shear produces important changes in the turbulence structure of shear layers. On strongly cambered turbomachinery blades turbulence may be nearly eliminated on convex surfaces, while on strongly concave surfaces, momentum and heat transfer by quasi-steady longitudinal vortices dominate the ordinary turbulence process. The addition of discrete coolant jets makes this spanwise periodic three dimensional flow very difficult to understand and predict. The present study focuses on quantitative wall heat flux measurements on the concave surface by using thin film platinum heat flux sensors without and with discrete hole film cooling. The row of holes is located at almost 1/3 chordal distance measured from the stagnation point. The effect of blowing rate and coolant temperature on the overall effectiveness of the cooling process is discussed. The blowing rate of the discrete coolant jets along a concave surface is particularly important. When the blowing rate is small, the coolant jets act only as boundary layer tripping elements and almost no reduction in heat transfer is obtained. The present experiments are mainly performed at quite high blowing rates (m = 1.74 . . . 4.23). The current heat transfer data shows that, at high blowing rates, the coolant jets strongly penetrate into the mainstream and attach at about 10 hole diameters downstream of the ejection holes. The strong jet penetration and reattachment enhances the turbulent mixing levels near the ejection site. The study also deals with the numerical predictions of convective heat transfer rates on the concave surface without coolant film ejection. Measured heat transfer coefficients and the predictions taking into account the influence of streamwise concave curvature are compared.

* Member AIAA
Assistant Professor of Aerospace Engineering
Previously: von Karman Institute for Fluid Dynamics, Turbomachinery Department
Ch. de Waterloo, Rhode Saint Genese, 1640
BELGIUM

LIST OF SYMBOLS

Symbols

$\bar{c}$	blade chord
d	coolant hole diameter
$\bar{d}$	exit hole diameter of the shaped hole
h	convective heat transfer coefficient $\dot{q}/(T_{\infty o} - T_w)$
k	thermal conductivity
Ma	Mach number
ℓ	mixing length
m	local blowing rate $\rho_c U_c / \rho_\infty U_\infty$
$\dot{m}$	mass flow rate
Nu	Nusselt number $h\bar{c}/k$
p	static pressure
Pr	Prandtl number
Re	Reynolds number $\rho U_\infty \bar{c}/\mu$
s	curvilinear coordinate measured from stagnation point negative on the pressure side
T	temperature
TU	free stream turbulence intensity
U	velocity
u'	fluctuating velocity

Subscripts

c	coolant flow condition
ex	exit
∞	free stream flow condition
in	inlet
o	total condition with or without coolant injection
is	isentropic
r	recovery
w	wall

INTRODUCTION

The success of the thermal design of a high temperature gas turbine blade is closely related to good understanding of fluid dynamic mechanisms and reliable predictions of gas side convective heating rates occurring in the fluid layers surrounding the blade. Early work on the effects of curvature was carried out by Prandtl (1) and Wilcken (2). They were the first to show that various parts of the boundary layer are variously affected by centrifugal force in the presence of a curved surface. A concave surface produces a tendency to force the fast parts of the flow toward the surface and the slow parts away from it. This tendency encourages the exchange of the slow layers next to the surface with the faster layers on the inside of the mainstream inviscid flow. This exchange reinforces the already existing turbulence features of the flow developing on the strongly concave pressure side of a gas turbine blade. The existence of a round leading edge with a stagnation flow, the existence of a short distance with a strong convex curvature near the leading edge and a sudden curvature change from convex to concave are some common geometrical features of a turbine blade pressure side. The addition of cold, high density fluid layer originating from discrete inclined coolant jets also complicates the gas side heat transfer problem on the pressure side. There has been considerable amount of work performed on curvature effects on the hydrodynamics of duct and channel flows. Kreith (3) showed that the heat transport from a concave wall was considerably more than from a convex wall in a curved channel experiment. Thomann (4) measured the local heat transfer coefficient distribution on straight convex and concave surfaces in a supersonic air stream with Ma = 2.5. Heat transfer was increased about 20% on the concave wall and decreased about 15% on the convex wall, compared with the flat wall.

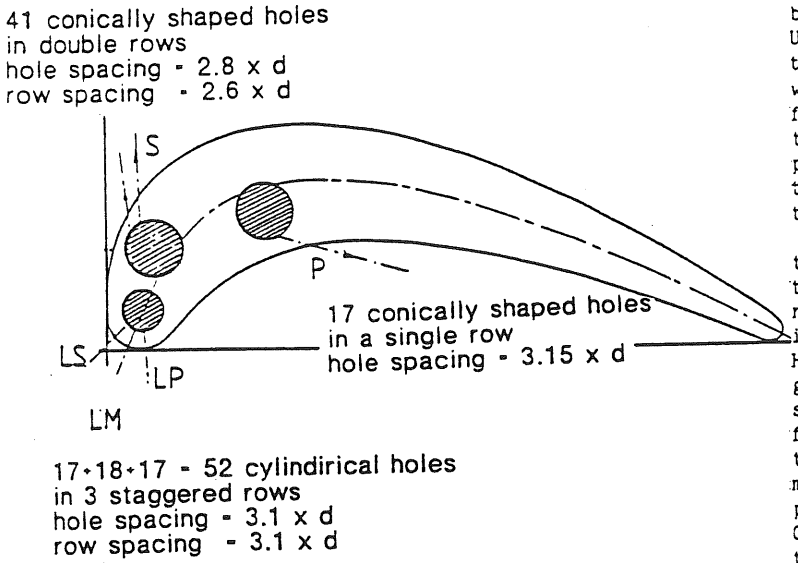

Figure 1.a

High pressure turbine rotor blade profile

According to Bradshaw (5) turbine blade heat transfer is mainly controlled by three dimensionality, streamwise curvature, Reynolds number, free stream turbulence, and unsteadiness. The three dimensionality occurs in the form of Taylor-Goertler vortices within the boundary layer. Mayle et al. (6) compared a concave, convex and flat surface from heat transfer point of view. They neglected the curvature of the turbine blade surface. They came to the conclusion that the only way curvature can affect the mean flow and thermal field is through the turbulent shear stress and turbulent heat flux generation mechanisms. A short duration heat

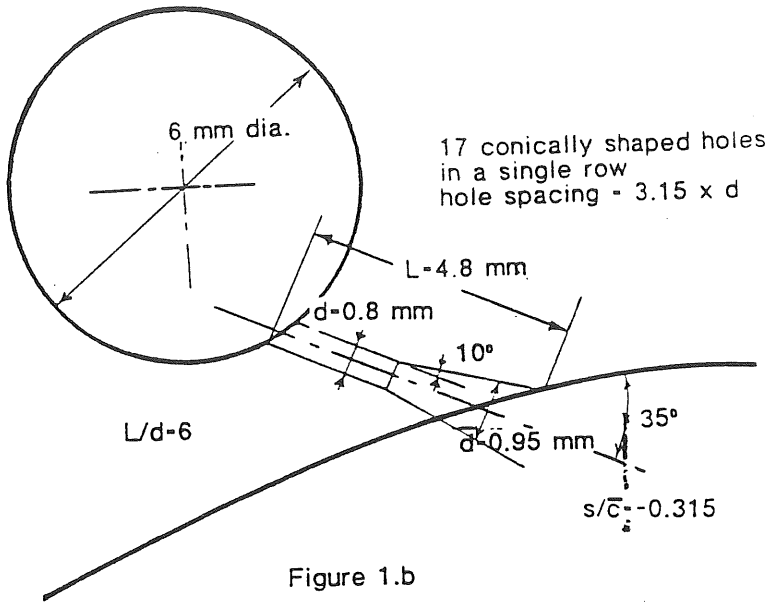

Figure 1.b

Discrete hole film cooling configuration on the pressure side

transfer study on a high pressure turbine rotor blade was performed by Daniels (7) in the Oxford University free piston tunnel under realistic gas turbine conditions. They found that the surface wall heating pattern was not strongly influenced from exit Mach number pattern. He interpreted this feature with the very small variation in the pressure surface Ma number distribution caused by the exit Ma number variations. He also noticed that at low Reynolds numbers, pressure side heat transfer is virtually uniform from $s/\bar{c} = -0.2$ up to the trailing edge. At higher Reynolds numbers, the pressure side heat transfer increases monotonically toward the trailing edge. He found that the concave side heat transfer at a given free stream turbulence level, depends strongly upon two counter-acting phenomena; the free stream acceleration tending to suppress transition and the instability generating mechanism of the concave curvature tending to promote transition and augment wall heating rates. Consigny and Richards (8) also reported similar trend for the concave side of a HP turbine rotor profile tested in a short duration heat transfer facility. Ito, Goldstein and Eckert (9) studied film cooling on both the suction side and pressure side of a gas turbine blade. They explained that suction side and pressure side coolant jets show different behaviors in terms of

providing a cold protective layer on the surfaces. They analytically showed that the radius of curvature of the ejected circular coolant jet is a strong function of the coolant to free stream momentum flux rate and the injection angle. They concluded that on a strongly concave surface when $I. \cos^2\alpha > 1$, the absolute value of the coolant jet radius of curvature becomes smaller than the radius of curvature of the wall showing the importance of the coolant momentum flux level in obtaining a protective coolant layer which is closely located near the concave wall. Decreasing the radius of curvature of the coolant film on a concave surface will improve the cooling effectiveness only if $I. \cos^2\alpha > 1$. Dring, Blair and Joslyn (10) carried out an experimental investigation of film cooling on a large scale turbine rotor blade profile representative of the first stage of a HP turbine. The data presented is one of the very limited number of sets including the effects of curvature and rotation simultaneously. They found a very large radial displacement of the coolant field during the visualizations. They attributed this feature to the radial component of the free stream flow over the blowing region. Their cooling effectiveness data on the pressure surface showed a much faster decay of the effectiveness than did the flat wall data because of curvature effects and rotation. Daniels (7) also performed a short duration study of film cooling on the concave surface of gas turbine blade in the Oxford University Engineering Laboratory. He reported a detrimental effect on the pressure side heat transfer rate because of film ejection on the pressure surface. His explanation of this detrimental effect was the existence of the coolant film acting as a boundary layer trip and forcing transition of the pressure surface boundary layer. As a matter of fact, very close to the ejection point, the coolant film may separate and the free stream may penetrate beneath it. The poor film cooling behavior was connected to the concave curvature and low coolant momentum flux on the pressure side. Pressure side heating rate measurements without and with film cooling on a turbine blade pressure side was performed by Horton, Schultz and Forest (11). They didn't report any transitional behavior on the concave surface when there is no cooling. The levels of heat transfer measured implied that the boundary layer is turbulent all over the concave surface. The heat flux sensors located around the leading edge detected the existence of a very small separation bubble very near the leading edge, and it was believed that the bubble tripped the pressure side boundary layer. They found no significant cooling performance for a wide range of blowing rates on the pressure side. They showed that the coolant fluid played no part in the development of the boundary layer at m = 1.5. It is likely that coolant air simply passed through the boundary layer and was sent in the mainstream, without coming back to the concave surface as a protective layer.

EXPERIMENTAL APPARATUS

Test Facility

A short duration technique was applied and use was made of the von Karman Institute isentropic compression tube facility. The operation principles of this facility were developed by Schultz et al. (12) about 16 years ago. The VKI CT-2 facility (Richards, 13) constructed in 1978, consists of a 5 m long, 1 m diameter cylinder containing a light weight piston, driven by the air of a high pressure reservoir. This cylinder is isolated from the test section by a fast opening slide valve. As the piston moves, the gas in front of it is nearly isentropically compressed until it reaches the pressure, and hence temperature levels defined by the tunnel operator. The fast opening valve is then actuated by means of a detonator, allowing this pressurized air to flow through the test section. Constant freestream conditions are maintained in the test section until the piston completes its stroke. The maximum test section dimensions are 250 x 100 mm^2. The freestream gas conditions can be varied between 300 and 600 K and 0.5 and 7.5 bar. A 5 m^3 dump tank allows downstream pressure adjustments between 0.1 and 4 bar. A full simulation of Reynolds numbers, Mach numbers, and freestream to wall temperature ratio is available in the test section of the rig. A cryogenic heat exchanger system, a temperature controlled hot oil bath and a medium pressure coolant reservoir system with a precision pressure control capability enables the user to adjust the coolant air ejection process for quantitative film cooling heat transfer measurements. This kind of measurement requires the precise knowledge of the coolant pressure and temperature in the coolant plenum chamber during a typical test with a total duration of 500 ms. Further details about this facility and its operating principles are described by Jones et al. (14); Richards (13); Schultz et al. (15); Ligrani et al. (16); Consigny and Richards (8).

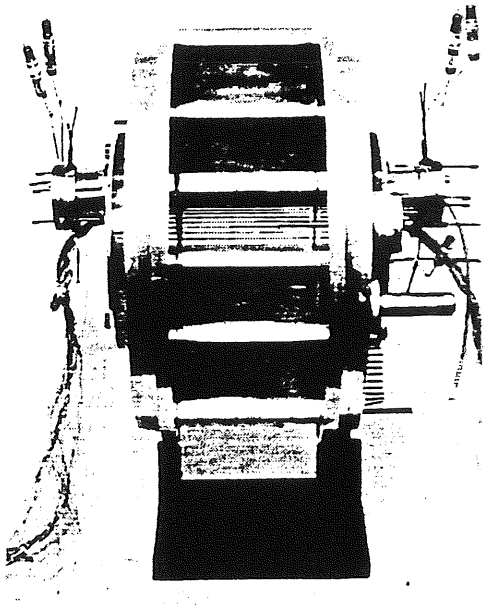

Figure 2

Heat transfer blade in the linear cascade

The Model

All measurements reported in this study were carried out on the same rotor blade section as tested by Camci and Arts (17), (18), (19). The cascade geometry is fully described in Consigny and Richards (8) and the cooling configuration is summarized in Fig. 1.a. Two staggered rows of shaped holes (d = 0.88 mm, $s/\bar{c}$ = 0.206, 0.237) are located on the suction side (row S); the row and hole spacing are respectively 2.48 mm and 2.64 mm, Fig. 1.a. The same model also carries a leading edge (LS, LM, LP) showerhead cooling arrangement. The leading edge and suction side cooling holes are blocked internally for the current investigation. However, the coolant hole pattern on these locations continues to act as surface roughness elements although the plenum chambers are filled with an internal blockage material. Fig. 1.b shows the details of the pressure side ejection site with a single row of 17 conically shaped cooling holes. The row is located at $s/\bar{c}$ = -0.31 and the length to diameter ratio is about 6. The coolant flow is supplied by a regenerative type cryogenic heat exchanger allowing a correct simulation of the coolant to freestream temperature ratio. Pressure tappings and miniature thermocouples provide continuously the coolant characteristics. The blade instrumented for heat flux measurements was milled from "Macor" glass ceramic and 45 platinum thin films were deposited on its surface.

Freestream Turbulence Generation

The heat transfer blade is one of the six blades located in a linear cascade as shown in Fig. 2. The freestream turbulence was generated by a grid of spanwise oriented bars. The turbulence intensity was varied by displacing the grid upstream of the model; a maximum of 5.2% was obtained. The natural turbulence intensity of this facility is about 0.8%.

Data Acquisition

All the pressure, temperature, and heat flux measurements were directly acquired by a PDP 11 based high speed data acquisition system. The details of this system with a total sampling rate of 500 KHz is given by Camci et al. (19); Camci (20); Camci and Arts (17); and Camci and Arts (18).

Measurement Technique

The local wall heat flux is deduced from the corresponding time dependent surface temperature evolution, provided by the thin films. The wall temperature/wall heat flux conversion is obtained from an electrical analogy, simulating a one dimensional semi-infinite body configuration. A detailed description of this transient technique is given by Schultz and Jones (12); Ligrani et al. (21). The convective heat transfer coefficient is defined as the ratio of the measured wall heat flux and the difference between the freestream recovery and the local wall temperatures. A recovery factor equal to 0.896 is used, as if the boundary layer on the blade surface was turbulent elsewhere. The uncertainties on the different quantities measured have been estimated as follows:

h = 1000 W/m^{2}K ± 50 W/m^{2}K
P = 2200 mmHg ± 15 mm Hg
T = 100 C ± 0.5 C
$\dot{m}_c$ = 0.020 kg/s ± 0.0005 kg/s
m = 0.96 ± 0.03

A baseline check on the heat flux measurement technique was performed by measuring Stanton number distributions on a flat plate with and without a favorable pressure gradient. For the zero pressure gradient case, the free stream Mach number was about 0.42 all over the plate. For the experiment with favorable pressure gradient, the free stream Mach number was

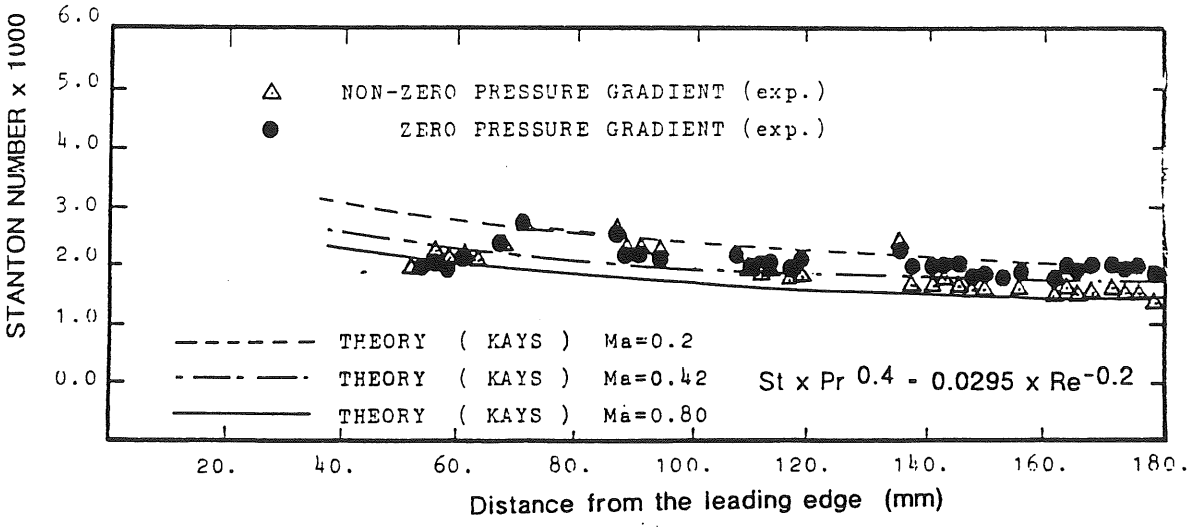

Figure 3

Measured and predicted Stanton number distribution over the flat plate without coolant injection

A baseline check for wall heat flux measurements

smoothly increasing from 0.20 to 0.80. A comparison of the measured data with an available heat transfer correlation from Kays (22) is shown in Fig. 3. The data agree with the equation with a maximum deviation of 5 percent. The experimental uncertainty of the Stanton number data shown in Fig. 3 based on a 20:1 confidence level is estimated to be ± 8 percent.

EXPERIMENTAL RESULTS AND DISCUSSION

Blade Velocity Distribution

The measured isentropic Mach number distributions along the blade surfaces at zero incidence are shown in Fig. 4. The Mach number at the inlet of the cascade was measured to be 0.25, at one chord length upstream of the passage. On the suction side, between the stagnation point and $s/\bar{c}$ = 0.05, the mainstream accelerates to Ma = 0.3 5. This favorable pressure gradient region continues up to $s/\bar{c}$ = 0.30 and between $s/\bar{c}$ = 0.30 and 0.45, a flat region is observed. Further downstream, the mainstream continues to accelerate and almost sonic velocities occur near the trailing edge. On the pressure side, following the strong acceleration around the leading edge, a maximum velocity takes place around $s/\bar{c}$ = -0.05. A diffusion region is observed along a very short distance between $s/\bar{c}$ = -0.08 and -0.12. The position where the curvature changes from convex to concave and the onset of the deceleration appear to be almost at the same position. Starting from $s/\bar{c}$ = -0.30, a favorable pressure gradient accelerates the mainstream up to nearly sonic velocities near the trailing edge. A two dimensional, finite area, time marching method, developed by Arts (23) has been applied to predict the inviscid free stream flow in the cascade. The prediction at zero incidence shown in Fig. 4 agree well with the measured data. Since this method does not accurately model the leading edge flow, a singularity method was found to be more eligible for the computation of the inviscid free stream velocities around the leading edge and for an accurate determination of the stagnation point position. The details of this prediction is given in (17). Singularity predictions near the leading edge asymptotically approach the finite area computations and the measured Mach number data as shown in Fig. 4. As a result of singularity calculations, the stagnation point at zero incidence has been found to be at $s/\bar{c}$ = -0.019. The pressure side boundary layer starts to grow along a smooth surface between the stagnation point and the cooling row LP shown in Fig. 1.a. The cooling row LP at $s/\bar{c}$ = -0.026 appears as a surface roughness for the pressure side boundary layer.

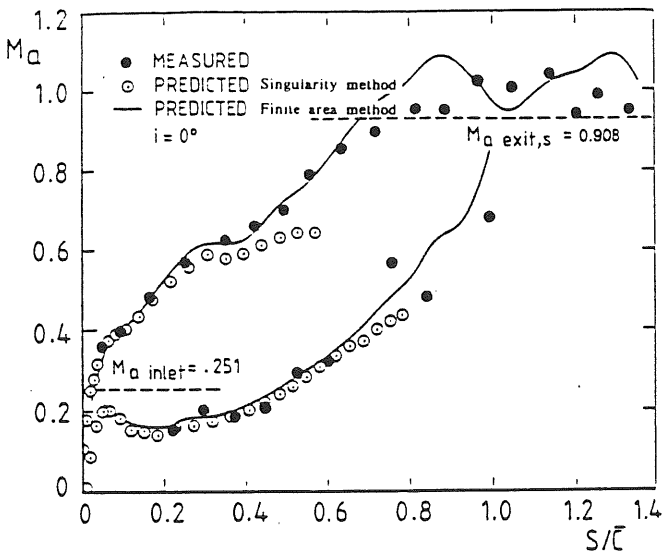

Figure 4

Blade velocity distribution

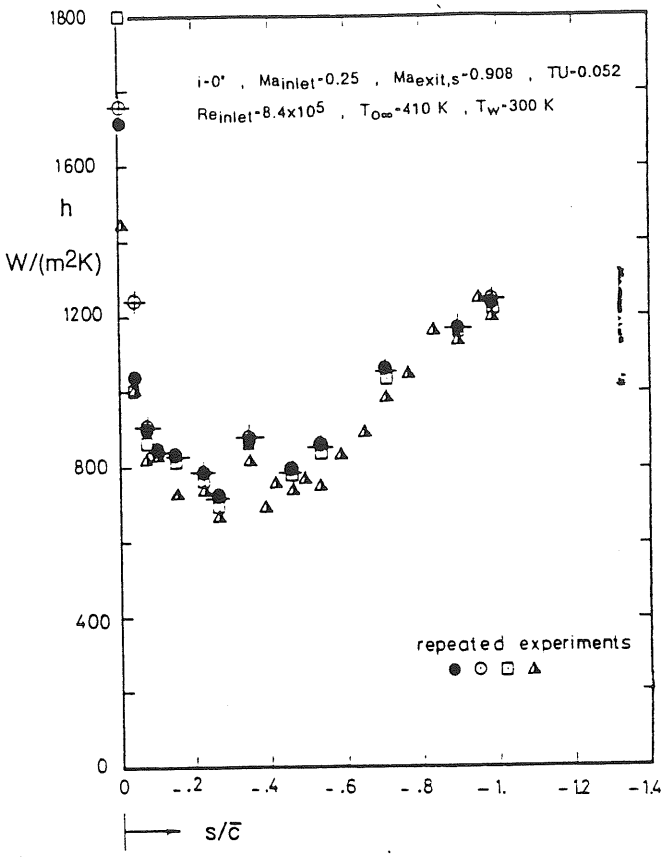

Figure 5

Pressure side heat transfer without coolant ejection

Pressure Side Heat Transfer Without Film Cooling

Measured convective heat transfer coefficient distribution on the concave side of the blade is given in Fig. 5. Four repeated experiments performed at different times are shown for an exit Mach number of 0.92. The free stream turbulence intensity for the experiment was always kept about 5.2%. Highest heating rates occurred near the stagnation point. Minimum heat transfer coefficient levels occurred

near $s/\bar{c}$ = -0.30 where the single row of holes are located. Just downstream of the row of cooling holes at $s/\bar{c}$ = -0.31 a sudden increase of at least 25% in heat transfer coefficient was observed. This elevated level was attributed to the fact that the existence of non-ejecting rows induce flow separation and immediate reattachment of this extremely thin boundary layer. During the experiments, the plenum chamber which was normally feeding this specific row of holes was carefully blocked. After $s/\bar{c}$ = -0.31 the heat transfer coefficient increased monotonically just like the increase in the freestream velocity in the streamwise direction.

The influence of the concave curvature on heat transfer is possibly enhanced by the existence of a stagnation point (leading edge flow) just upstream of the strongly concave region where $-0.10 < s/\bar{c} < 0$. The vortices with streamwise vorticity vectors parallel to the main flow direction are known to be closely spaced near the stagnation point. The amount of heat transfer in this area is proportional with the spacing of these vortices. The complicated flow field originating from the stagnation point is expected to break down when the curvature inversion occurs near downstream of the leading edge at about $s/\bar{c}$ = -0.08. The curvature distribution for the entire pressure side is given in Fig. 6. After the change of curvature, the boundary layer continues to develop on a highly concave surface. In the past, it was a well documented fact that the turbulent length scale was increased on concave surfaces, resulting in enhanced wall heating rates when compared to flat walls. The simultaneous influence of the leading edge flow and the strong concave curvature makes the prediction of heat transfer relatively difficult in comparison to the flow on a concave wall with no round leading edge (sharp leading edge). Because of the highly accelerating nature of the mainstream flow after $s/\bar{c}$ = -0.2 as shown in Fig. 4, a laminarization process depending upon the pressure gradient parameter ($K = \frac{\nu}{U_\infty^2} \cdot \frac{dU_\infty}{dx}$) is expected. Laminarization in a favorable pressure gradient reduces the wall heating rate in contrast to enhancements resulting from the interaction of the leading edge flow and the concave curvature of the pressure side.

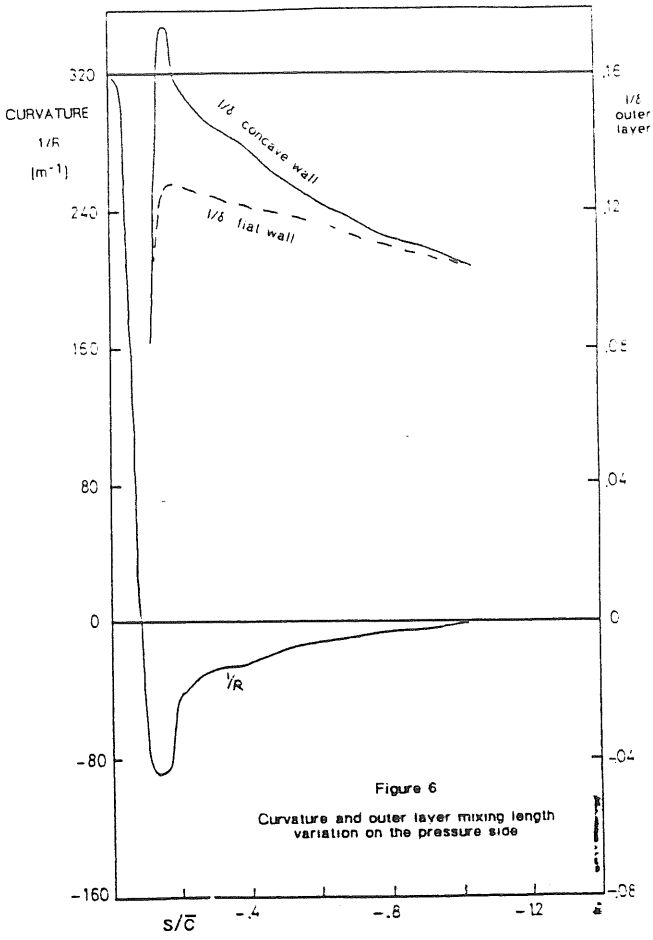

Figure 6
Curvature and outer layer mixing length variation on the pressure side

Numerical Prediction of Heat Transfer on the Pressure Side without Coolant Ejection

A numerical prediction of the wall heating rates along the pressure side was attempted by using a two dimensional differential boundary layer code, Crawford (24). A concave curvature model for the mixing length was implemented into the code. The influence of streamwise curvature on convective heat transfer was described using the turbulent mixing length variation as suggested by Bradshaw (25) and So (26). The mixing length variation was described as follows:

$$\frac{\ell}{\ell_o} = (1 - \frac{1}{2}\beta \cdot Ri)^{3/4}$$

where $Ri = S_c \cdot (1 + S_c)$ and

$$S_c = \frac{2 \cdot \frac{U}{R}}{\frac{\partial u}{\partial y}}$$

where $\beta = 6$

The velocity peak downstream of the stagnation area $s/\bar{c}$ = -0.08 was found as the prime cause of the appearance of a zone with flow reversal in the boundary layer. The velocity profile was therefore artificially flattened in this region in order to avoid numerical problems arising during the calculation process with the specific method. As a matter of fact, the boundary layer method available was not able to treat reverse flow regions.

Stanton number predictions taking the concave curvatures into account are shown in Fig. 7. Since a precise determination of the onset of transition was difficult, a set of predictions in a range of transitional Re_θ from 10 to 200 were evaluated and compared with the measured data. The computed momentum thickness Re number distributions shown in the figure indicate relatively lower Re_θ values on the pressure

side when compared to the suction side. Re_θ has a value of about 100 near the curvature inversion point. The best agreement with the measured Stanton number data was found when transitional calculations were triggered in a range between Re_θ = 10 and Re_θ = 100. The predictions performed at Re_θ = 150, 175 and 200 resulted in greater discrepancies in comparison to the measured data. As shown in Fig 7, predictions with Re_θ = 150, 175 and 200 indicate relatively large laminar zones on the forward portion of the pressure side. The prediction for downstream of the leading edge ($|s/\bar{c}| > 0.7$) showed good quantitative agreement with the measured data, regardless of the choice of the onset of transition point. The discrepancy between the data and the present calculation is quite large, especially in the first half of the pressure surface. It is very much likely that a more complex flow structure is existing in this zone than the flow numerically simulated by the differential equation and the turbulence model used in the predictions.

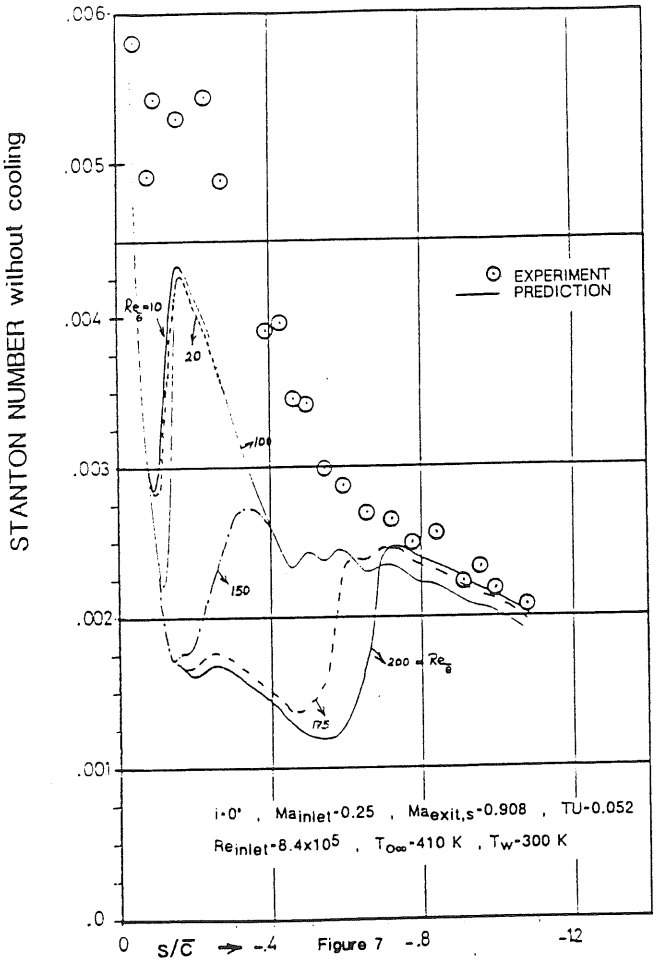

Figure 7

Measured Stanton number distribution and comparison with predictions on the pressure side

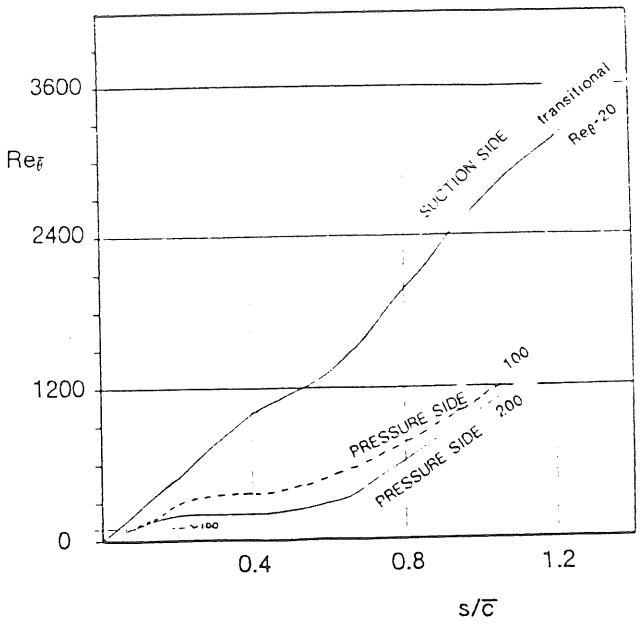

Figure 8

Momentum thickness Re variation on the pressure side and comparison with the suction side data

Pressure Side Heat Transfer with Coolant Ejection

Downstream of Single Row of Holes at $s/\bar{c}$ = -0.31

The coolant ejection geometry of location P_{ss} as shown in Fig. 1.b was designed to supply high blowing rate coolant. It is a proven fact that coolant jets on concave surfaces have a tendency to move closer to the wall (or reattach) when the coolant momentum flux $I \cos^2\alpha$ is greater than unity. The present film cooling experiments were carried out in a high blowing rate range varying between m = 1.74 and 4.23. Low blowing rate experiments (m = 1.74) were not included in the program mainly because of the past work showing only a detrimental effect from the coolant jets. The weak jets are known to trip the boundary layer and augment wall heating rates near

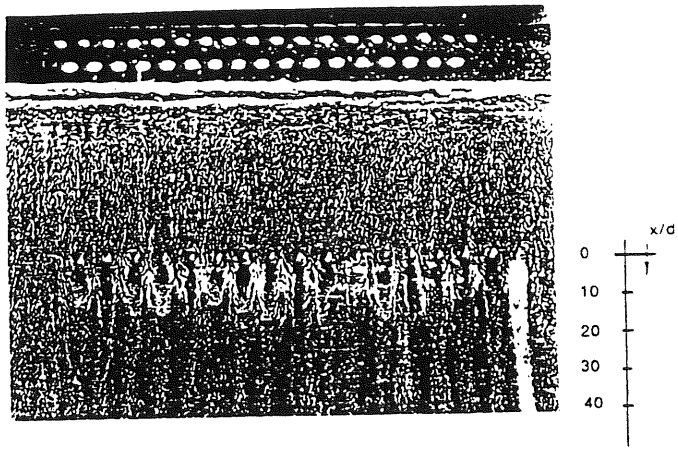

Figure 9

Surface oil flow visualization of film cooling on the pressure side

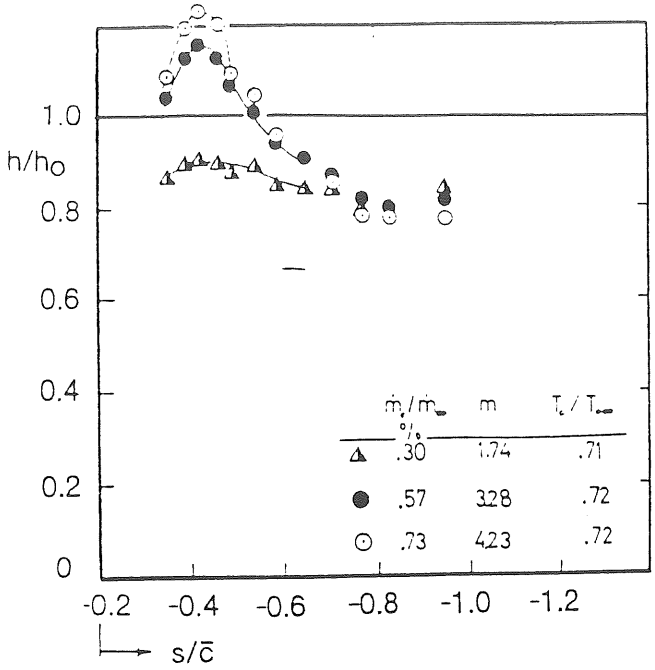

Figure 10

Effect of blowing rate on the pressure surface wall heating rate , T_c-0.72 x $T_{o\infty}$

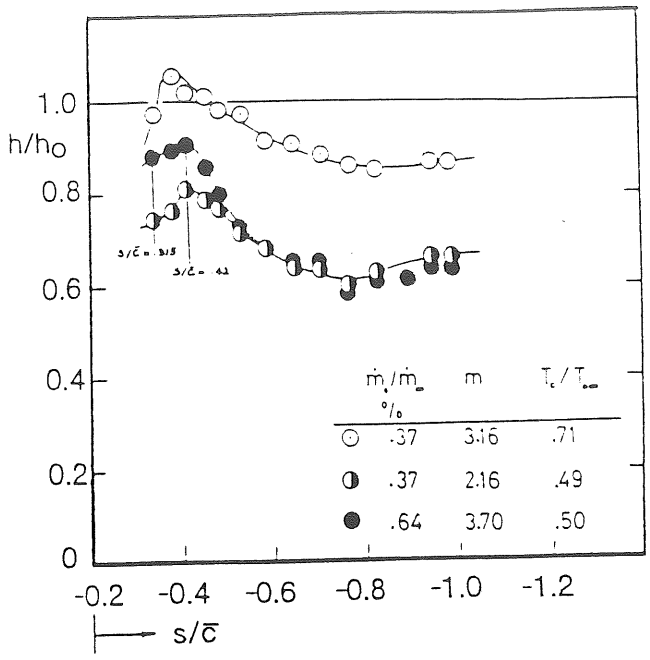

Figure 11

Effect of blowing rate on the pressure surface wall heating rate , T_c-0.50 x $T_{o\infty}$ (actual coolant temperature ratio)

downstream of the hole rather then reducing h/h_o values. The experiments were performed at two very typical coolant temperature levels, at 0.70 x $T_{o\infty}$ and 0.50 x $T_{o\infty}$. Further details of the heat transfer data sets without and with film cooling are given in Table 1.

A surface oil flow visualization on the concave side of the blade is shown in Fig. 9. The visualization included the near leading edge region and the downstream of the single row of holes located at $s/\bar{c}$ = -0.31. An oil accumulation region near the leading edge indicates a very small separation bubble at about $s/\bar{c}$ = -0.10. The bubble location is consistent with inviscid flow calculations. The calculated and measured pressure side Ma number distribution as shown in Fig. 4 indicates a deceleration zone after a velocity maximum near the leading edge at about $s/\bar{c}$ = -0.10. The uniformity of the coolant jets in the spanwise direction was also checked using the same flow visualization technique. Surface oil flow patterns showed that the spanwise uniformity of the 11 central holes (out of 17) was excellent. Fig. 9 was produced at a blowing rate of m = 1.74, T_c = 0.71 x $T_{o\infty}$.

The effect of blowing rate on the surface heating rate at a coolant temperature of 0.72 x $T_{o\infty}$ is shown in Fig. 10. At the lowest blowing rate of m = 1.74, a 15% heat transfer coefficient reduction from non-cooled case was observed. When the blowing rate was increased, the discrete jets tended to penetrate into the freestream; however, with the strong concave curvature, they are forced to come close to the surface at about 10 hole diameters downstream of the row. The maximum h/h_o values occurring at x/d = 10 in Fig. 10 are directly related to the coolant jet reattachment as expected at high blowing rates when I $\cos^2\alpha$ > 1. The increase in heat transfer coefficient ratio h/h_o before x/d = 10 could also be attributed to the unprotected, nearly triangular zones between discrete coolant holes in a row. Increasing the blowing rate to m = 4.23 significantly augmented the near hole heat transfer coefficient peak occurring at about x/d = 0.10. At T_c = 0.71 x $T_{o\infty}$, the blowing rate only affected the first 40 hole diameter downstream of the row. After 40 diameters distance, h/h_o values did not change significantly with the blowing rate.

In an actual gas turbine environment, the present day coolant temperature level is lower than 0.71 x $T_{o\infty}$. The coolant temperature levels of about 0.50 x $T_{o\infty}$ are very common. In order to investigate the influence of the blowing rate on h/h_o at this more realistic temperature level, a cryogenic heat exchanger controlled cold air supply was connected to the plenum chamber of the pressure side coolant ejection row. Since the total temperature in the freestream was about 410°K, a coolant temperature level of 205°K was needed. The h/ho values were significantly enhanced when the blowing rate was increased from m = 2.16 to 3.70 in the near hole region, as shown in Fig. 11. However, the coolant jet penetration and reattachment zone was limited to a shorter downstream distance of about 20 hole diameters. The blowing rate dominated h/h_o zone was reduced from 40 hole diameters to 20 diameters by decreasing the coolant temperature

from 0.70 x $T_{o\infty}$ to 0.56 x $T_{o\infty}$. After reattachment, the h/h_o curve was not significantly altered by the blowing rate (x/c > 20), Fig. 11. The present cooling geometry provided about an average 35% heat transfer coefficient reduction from the non-cooled value in this region. For the current blowing rate range (m = 3.12 . . . 3.70) reducing the the coolant temperature level from 0.70 x $T_{o\infty}$ to 0.50 x $T_{o\infty}$ provided at least a 20% gain of h/h_o in the region where blowing rate influence was minimal (x/d > 20). The near hole region heating rates were dominated by the unprotected zones between the cooling holes in the row.

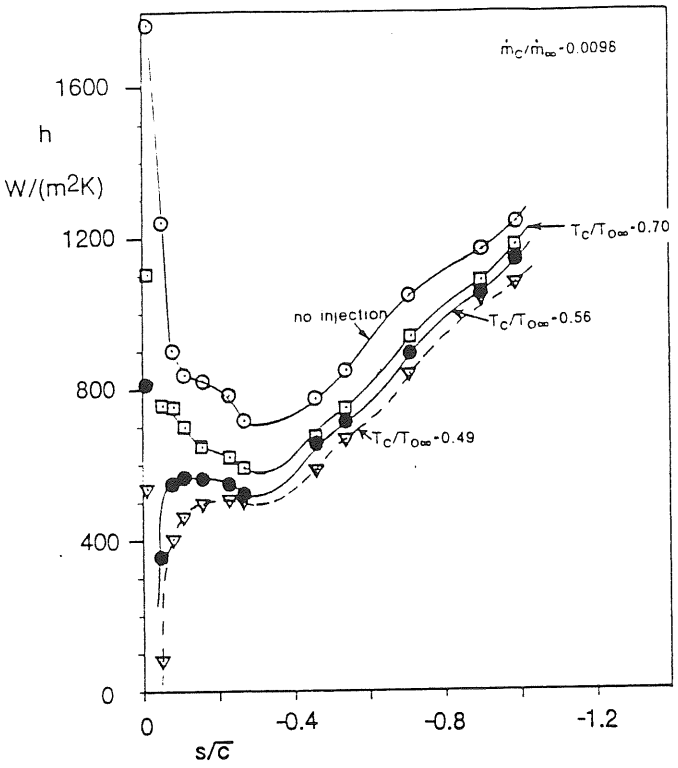

Figure 12

Effect of coolant ejection from the leading edge on the pressure side heat transfer

Superposition of the Pressure Side Film Cooling and Leading Edge Film Cooling

The coolant jets issued from a mid pressure side location are very much likely to interact with coolant layers already introduced around the leading edge, e.g., shower head cooling configuration. This part of the experimental program was designed to observe if there was a significant contribution of coolant jets issued from the leading edge on the pressure side cooling region downstream of $s/\bar{c}$ = -0.31. The first group of experiments was conducted with only leading edge film cooling at various coolant temperatures with a constant coolant to freestream mass weight ratio of $\dot{m}_c/\dot{m}_\infty$ = 0.98%. It was assumed that the total coolant flow was about 3% for the blade and one third of this amount was consumed at the leading edge location. Fig. 12 shows significant reductions in heat transfer coefficient h all over the pressure side. The most significant protection occurred in the first 40% of the chord length. However, downstream of the $s/\bar{c}$ = -0.40 location always had a slight protection effect depending on the coolant temperature level. It was expected that this coolant blanket effect from the leading edge ejection location would improve the pressure side cooling scheme already discussed in Figs. 9, 10 and 11.

Fig. 13 includes the results from two experiments on the pressure hole, one with only pressure side ejection from row P, another experiment with both pressure side ejection and leading edge shower head cooling (LS + LM + LP). Both experiments were performed at the same coolant temperature level. The local blowing rates were also kept at the same level of m = 4.2 on the location P at $s/\bar{c}$ = -0.31. Fig. 13 shows that there is an important contribution of the leading edge films on the pressure side heat transfer rate reduction downstream of $s/\bar{c}$ = -0.31. This contribution would be attributed to the fact that the film originating from location P sees a turbulent approaching boundary layer already containing some coolant fluid. Ejection into this already thickened protection layer at location (P) results in a better wall protection compared to the case where leading edge holes were blocked, Fig. 13. The success of the superposition entirely depends upon the way the jets are introduced on the blade surface near the leading edge. The superposition on the pressure side may provide at least a 15% gain on non-dimensional heat transfer coefficient h/h_o on the pressure side provided that the showerhead configuration generates smooth and effective coolant layers in the first 40% chordal distance on the pressure side.

A complete heat transfer simulation of a film cooling process on the HP blade described in Fig. 1.a is shown in Fig. 14. Details of the leading edge (LS + LM + LP), pressure side (P) and suction side (S) cooling geometries are given in references (18), (17), and (19). The three experiments shown in the figure were performed at total coolant to freestream mass weight ratios of 0.93, 2.07 and 3.09% at a fixed coolant temperature of 0.70 x $T_{o\infty}$. At the lowest mass weight ratio of 0.93, the jet penetration and reattachment feature in the near hole zone of the pressure side (downstream of $s/\bar{c}$ = -0.31) did not exist. The h/h_o peak became more visible at $\dot{m}_c/\dot{m}_\infty$ = 2.07% in the first 20 hole diameters distance downstream of the row P. Increasing total coolant flow to 3.09% clearly augmented h/h_o in the near hole region. However, increasing blowing rates provided better protection after the first 20 hole diameter region downstream of the row P. Higher blowing rates provided better wall protection at near downstream of the row, however near downstream h/h_o values were augmented.

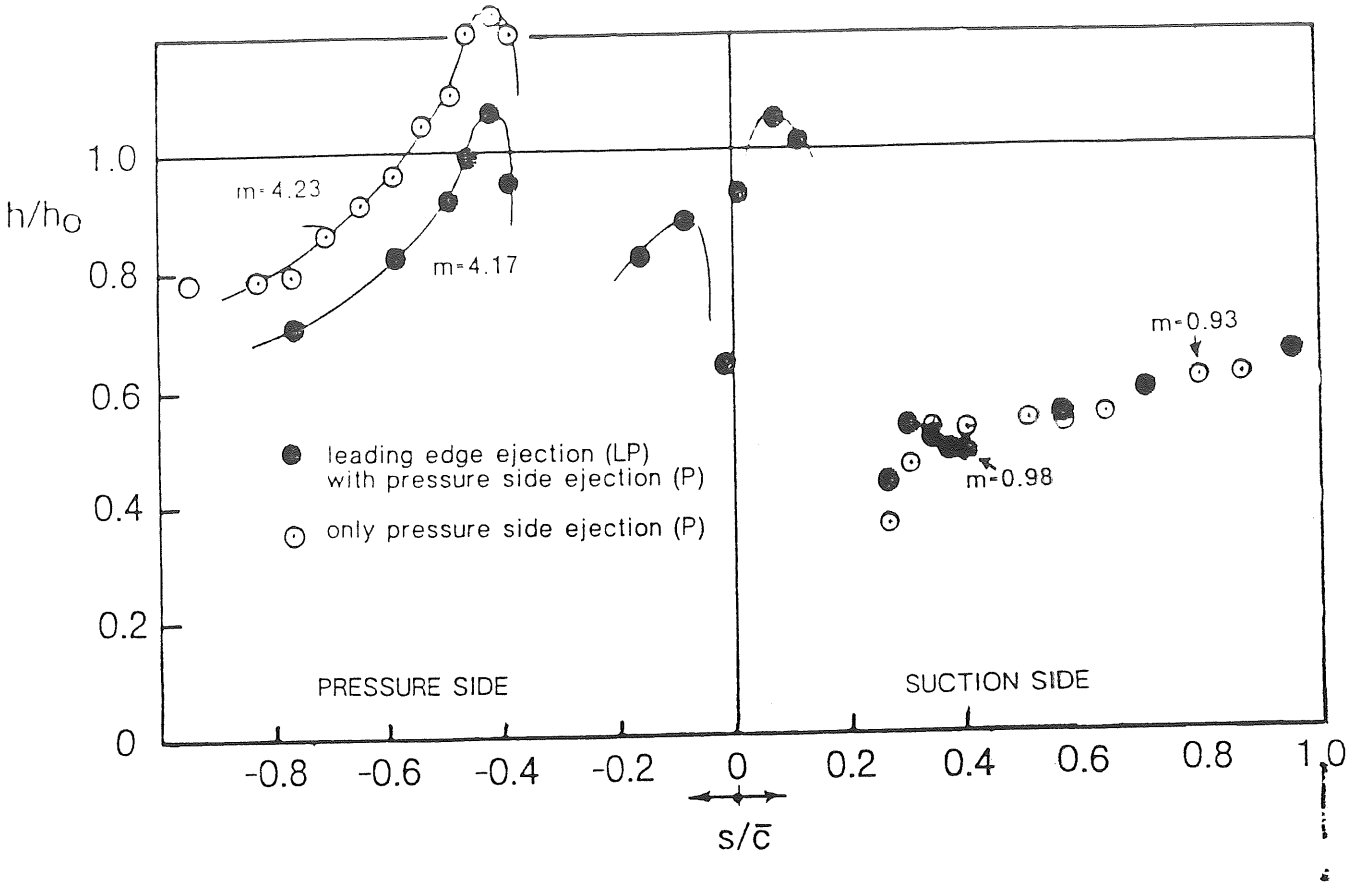

Figure 13

Superposition of pressure side film cooling
and leading edge film cooling

CONCLUSIONS

A detailed short duration heat transfer study of discrete hole film cooling on the concave surface of a high pressure turbine blade was presented. The heat transfer without film cooling on the concave surface was predicted using a two dimensional differential boundary layer method, taking into account the strong concave curvature. The discrepancy between the data and the present calculation is quite large, especially in the first half of the pressure surface. Film cooling experiments were focused on the high blowing rate zone above m = 1.70. At high blowing rates the discrete jets tended to penetrate into the free stream. Maximum h/h_o values occurred almost at 10 hole diameters downstream of the cooling row. This maximum in h/h_o was attributed to coolant jet reattachment. Realistic coolant temperature levels (0.50 x $T_{o\infty}$) significantly reduced overall h/h_o levels when compared to experiments with T_c = 0.70 x $T_{o\infty}$. Pressure side jets ($s/\bar{c}$ = -0.31) provided a better wall protection when a leading edge showerhead cooling was superposed on the concave surface.

ACKNOWLEDGEMENT

The experimental part of this study was completed in the von Karmam Institute for Fluid Dynamics. The author acknowledges the continuous support of Professor T. Arts and Professor F.A.E. Breugelmans during his past work at the V.K.I.

References

1. Prandtl, L., "Sonderdruck aus Vortnage aus dem Gebiete der Aerodynamik and Yeryandter Gebiete," Aachen (available in English as NACA Techanical Memorandum No. 625).

2. Wilcken, H., "Turbulente Grenzchichten an Gewolbten Flachen," Berlin, Vol. 1, No. 4, Sept. 1930 (available in English as NASA TT-F-11, 421, Dec. 1967).

3. Kreith, F., "The Influence of Curvature on Heat Transfer to Incompressible Fluids," Transactions of the ASME, Nov. 1955.

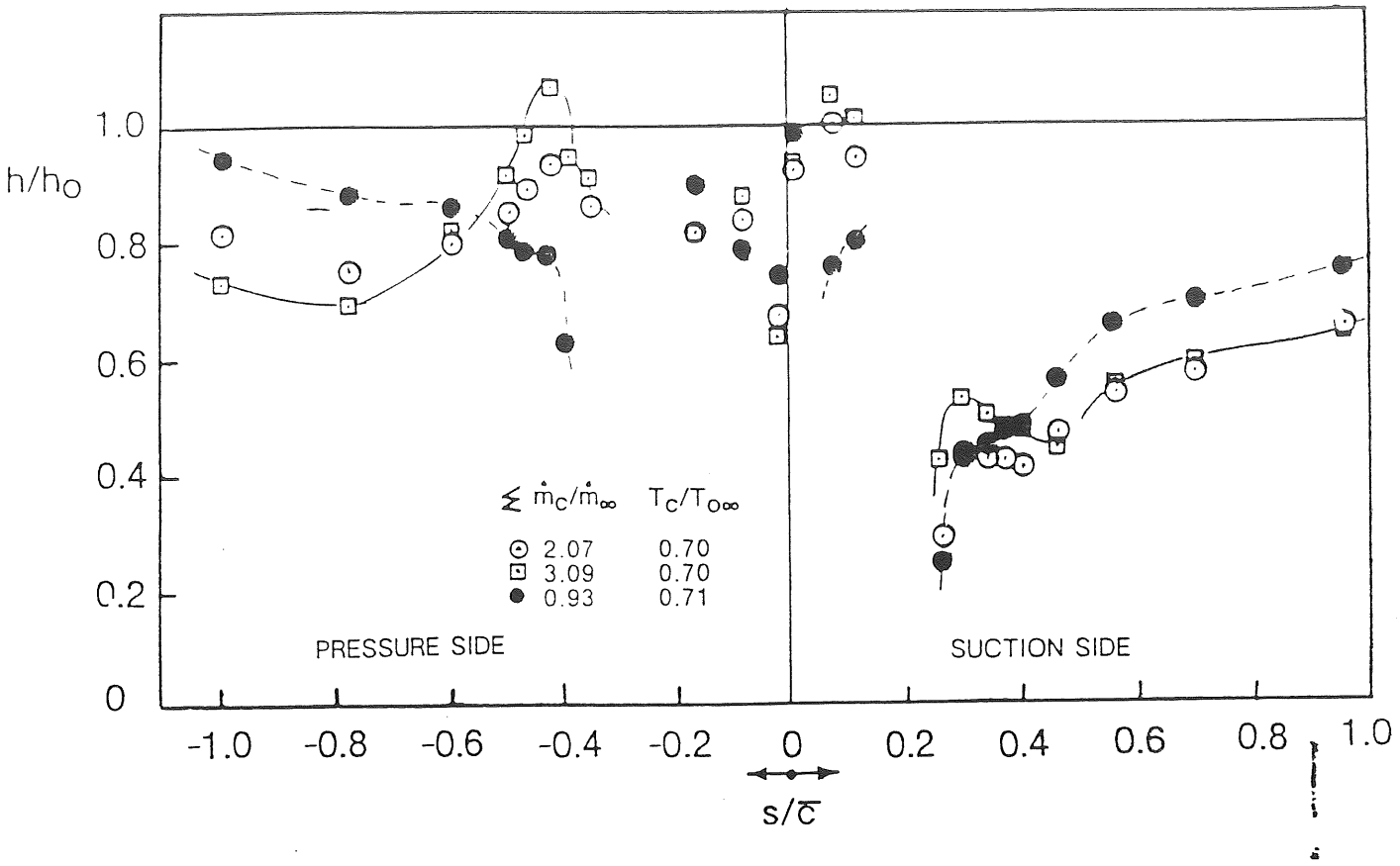

Figure 14

A complete heat transfer simulation of a film cooling process on the HP rotor blade

4. Thomann, H., "Effect of Streamwise Wall Curvature on Heat Transfer in a Turbulent Boundary Layer," Journal of Fluid Mechanics, 33, Part 2, pp. 283-292, 1968.

5. Bradshaw, P, "Effects of Streamwise Curvature on Turbulent Flow" AGARDograph, No. 169, 1972.

6. Mayle, R.E., Blair, M.F., and Kopper, F.C., "Turbulent Boundary Layer Heat Transfer on Curved Surfaces," Journal of Heat Transfer, Vol. 101, No. 3, Aug. 1979.

7. Daniels, L.C., "Film Cooling of Gas Turbine Blades," Ph.D. Thesis, Department of Engineering Science, University of Oxford, England, 1978.

8. Consigny, M., Richards, B.E., "Short Duration Measurements of Heat Transfer Rate to a Gas Turbine Rotor Blade," ASME Journal of Engineering for Power, V. 104, No. 3, July 1982, pp. 542-551.

9. Ito, S, Goldstein, R.J., Eckert, E.R.G., "Film Cooling of a Gas Turbine Blade," ASME Journal of Engineering for Power, Vol. 60, No. 3, July 1978, pp. 476-481.

10. Dring, R.P., Blair, M.F., Joslyn, H.D., "An Experimental Investigation of Film Cooling on a Turbine Rotor Blade," ASME Journal of Engineering for Power, V. 102, Jan. 80, pp. 81-87.

11. Horton, F.G., Schultz, D.L., Forest, A.E., "Heat Transfer Measurements with Film Cooling on a Turbine Blade Profile in Cascade," ASME paper 85-GT-117.

12. Schultz, D.L. and Jones, T.V., "Heat Transfer Measurements in Short Duration Supersonic Facilities," AGARDograph no. 165, 1973.

13. Richards, B.E., "Heat Transfer Measurements Related to Hot Turbine Components in the von Karman Institute Hot Cascade Tunnel," AGARD Conference Proceedings, No. 281, Testing and Measurement Techniques in Heat Transfer and Combustion, Brussels, 1980.

14. Jones, T.V., Schultz, D.L., and Hendley, A.D., "On the Flow in an Isentropic Free Piston Tunnel," A.R.C. R & M 3731, 1973.

15. Schultz, D.L., Jones, T.V., Oldfield, M.L.G., and Daniels, L.C., "A New Transient Facility for the Measurement of Heat Transfer Rates," in High Temperature Problems in Gas Turbine Engines, AGARD CP 229, Paper 2, 1977.

16. Ligrani, P.M., Camci, C., and Crawy, M.E., "Thin Film Heat Transfer Gauge Construction and Measurement Details," von Karman Institute Technical Memorandum No. 33, 1981.

17. Camci, C. and Arts, T., "Experimental Heat Transfer Investigation Around the Film Cooled Leading Edge of a High Pressure Gas Turbine Rotor Blade," J. of Engineering for Gas Turbines and Power, Vol. 107, No. 4, pp. 1016-1021, 1985.

18. Camci, C. and Arts, T., "Short Duration Measurements and Numerical Simulation of Heat Transfer Along the Suction Side of a Gas Turbine Blade," J. of Engineering for Gas Turbines and Power, Vol. 107, No. 4, pp. 991-997, 1985.

19. Camci, C., Arts, T., and Bruegelmans, F.A.E., "Experimental Convective Heat Transfer Investigation Around a Film Cooled High Pressure Turbine Blade," presented at 7th AIAA Symposium on Air Breathing Engines, Beijing, China, 1985.

20. Camci, C., "Theoretical and Experimental Investigation of Film Cooling Heat Transfer on a Gas Turbine Blade," Ph.D. Thesis, von Karmam Institute of Fluid Dynamics and University of Leuven, Belgium, 1985.

21. Ligrani, P.M. and Camci, C., "Adiabatic Film Cooling Effectiveness from Heat Transfer Measurements in Compressible Variable-Property Flow," J. of Heat Transfer, Vol. 107, No. 2, pp. 313-320, 1985.

22. **Kays, W.M. and Crawford, M.E., "Convective Heat and Mass Transfer," Mc-Graw Hill, New York, 1980.**

23. **Arts, A. "Cascade Flow Calculations Using a Finite Volume Method," in "Numerical Methods for Flow in Turbomachinery, VKI LS 1982-05, Brussels, April 1982.**

24. Crawford, M.E. and Kays, W.M., "Stan 5, A Program for Numerical Computation of Two Dimensional Internal/External Boundary Layer Flows," Stanford University, Dept. of Mechanical Engineering, Thermosciences Division, Report HM T-23, December 1975.